

In Situ Computerized Optical Reflectivity Measurement System For Ion Implantation

Pieter L. Swart, *Member, IEEE*, Beatrys M. Lacquet, *Member, IEEE*, Michael F. Grobler, and Herzl Aharoni

Abstract—A computerized *in situ* optical reflectivity measurement system for the quantitative determination of material parameter changes of a substrate during the process of ion implantation, is presented. These changes are related to the extent and nature of the induced crystal disorder in the substrate. The system comprises an optical reflectometer, with data acquisition and signal processing capabilities. For each sample a case history of the implant is obtained in the form of a continuous graph of reflectivity vs. a desired implantation parameter (e.g., dose). Examples regarding the implantation of $^{31}\text{P}^+$, $^{40}\text{Ar}^+$, and $^{14}\text{N}^+$ are presented. Additional suggestions for further system development and applications are also made. Among the advantages of *in situ* measurements are the time-effort-expenses savings, higher yield of experimental data per sample, higher accuracy, repeatability, and various possibilities of process control.

I. INTRODUCTION

ION implantation and post implantation annealing are routinely used in semiconductor device and circuit manufacturing. It enables a controlled introduction of desired ion species into a target, usually a semiconductor substrate, under various predetermined conditions. By proper selection of species and implant conditions, as well as post implant annealing procedures, the implanted target material properties can be changed to achieve desired device characteristics. The impact of the energetic penetrating ions is, however, such that disorder is created in the implanted substrate. In the extreme case, the degree of disorder may lead to the amorphization of an entire continuous layer at or below the substrate surface. For device fabrication purposes, knowledge of whether or not such a state has been reached or approached is of prime importance because it can influence subsequent processing parameters. The objective of this work is to describe a simple, nondestructive, fast and inexpensive technique for the determination of the degree of disorder during the implant, and any subsequent restoration [1].

The experimental determination of the conditions which induce a significant degree of disorder up to the level of

amorphization in the material was already addressed by us [2]–[9], as well as by other workers [10]–[20]. This was done by a variety of methods, some of which are destructive (such as SIMS, RBS, TEM, etc.), and other techniques which are nondestructive and mainly optical in nature. In the last case reflectance and transmittance measurements in the ultraviolet, visible and infrared regions of the spectrum are employed. For a given substrate the damage is known to be a function of the implant parameters such as dose, dose-rate, energy and ion species. The changes in the optical parameters are also functions of the substrate conditions during the implant. Temperature, tilt angle, beam scan rate, as well as crystallographic orientation, the original resistivity and the intrinsic defect type and density come to mind. The disorder which gives rise to the optical changes occurs in a region located at or below the substrate surface, leaving the bulk of the substrate unchanged. With knowledge of the pre-implanted optical properties, the changes occurring in the properties of the superficial layers can be separated, yielding information regarding the nature and extent of the damage in the implanted substrate.

In this work the optical reflectivity, R , of the substrate at a fixed wavelength, is used to characterize the changes which take place in the substrate during implantation. Reflectance of the surface proved [2]–[13] to be quite a sensitive indicator of the structural changes. Temporal changes in the reflectivity are of particular interest since noticeable changes in R occur at the onset, built-up and formation of a continuous amorphous layer at or below the substrate surface [2]–[7]. The most dominant change in R occurs during the crystalline to amorphous transition which is manifested by a steep increase in R from the unimplanted and low dose value to a higher value of R which signifies the formation of a continuous amorphous layer. As annealing takes place R is gradually reduced to almost its original value, indicative of crystal order restoration [1].

As mentioned before, the determination of whether or not amorphization and/or annealing have occurred, is of importance in many device fabrication procedures. In the literature, methods used to determine the optical reflectivity include using a tungsten lamp [19], double beam spectrometer [20], laser [21], and techniques such as spec-

Manuscript received September 10, 1992. This paper was supported by research grants from the Foundation for Research Development and Rand Afrikaans University.

The authors are with Sensor Sources and Signal Processing Research Group, Materials Laboratory, Faculty of Engineering, Rand Afrikaans University, P.O. Box 524, Auckland Park, 2006, South Africa.

IEEE Log Number 9205351.

troscopic ellipsometry [13], differential reflectance spectroscopy [11], [13] and Raman scattering [14]. A disadvantage of many of these techniques is that the optical reflectance measurements reported are performed *after* the completion of the implant, and *outside* the target chamber. Consequently, the information regarding the time evolution of events occurring during the actual implant cycle of a particular sample, is lost. To obtain such information, graphs (reflectivity (R) versus dose (D), for example) have to be constructed using several samples, each implanted to a different dose and yielding only one data point on the graph [2]–[7]. In addition to being time consuming and expensive, inherent inaccuracies are caused by the assumption that all the samples for that graph were implanted under exactly the same conditions, which is difficult to ensure. Data scattering and resolution problems therefore arise, reducing the possibility to observe small changes for example. Other typical problems related to the above, will also be discussed.

The technique to measure the changes in the optical reflectivity presented here, overcomes the problems mentioned above and offers additional advantages. A computer controlled data acquisition system which is connected to the optical reflectometer provides facilities for automatic calibration, adjustable data capture rate, data storage, signal processing and graphics.

II. *IN SITU* MEASURING SYSTEM

A schematic diagram of the computerized optical reflectivity measuring system is given in Fig. 1, and consists of three main parts. Part 1 contains the existing implantation apparatus. Parts 2 and 3 are modifications added to the apparatus, namely an optical reflectometer (2) and a data acquisition and signal processing system (3). A 350-keV ion implanter was used. The end station is a stainless steel target chamber in which the substrates were mounted on a rotating disk. However, due to a modification to be described later, the substrate was moved to a new cylindrical Faraday cup which is appended to the existing end station. The ion beam passes through the regular end station through an opening and the implantation is performed in the far end of the Faraday cup. The ion beam current signal is relayed from the Faraday cup to the data capturing and signal conditioning system.

An optical reflectometer which was constructed for this system contains the light source and optics which direct 50% of a light beam via optical windows to and from the substrate which is in vacuum in the Faraday cup. The intensity of the attenuated laser light reaching the substrate is such that it does not induce changes in the probed surface, making it a nondestructive measurement. The other 50% of the light used in the measurement stays unchanged, and serves as a reference for the calculation of the reflectance by the computer, as will be shown later. The two beams are then sensed by two separate sensors. The photocurrents produced are transferred to the signal conditioner. The intensity of the reflected beam changes continuously during the implantation due to changes in

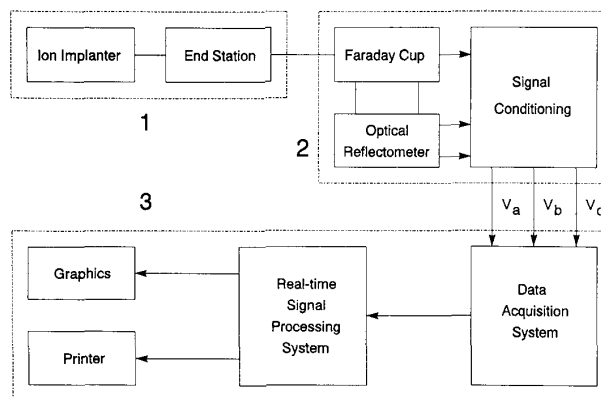


Fig. 1. A general block diagram of the system.

the substrate reflectivity. The signal conditioning system consists of three analog amplifier circuits which convert the above currents to voltages which are then sent to the data acquisition system. It also contains an analog filter for smoothing the ion beam current signal. The output of the signal conditioning system comprises three voltages: V_a , which represents the laser reference beam; V_b , the changing reflected light; and V_c which represents the ion beam current signal. These voltages are transferred to the data capturing and signal processing system, indicated as part 3. This system includes a data acquisition facility, a real-time signal processing unit, and data presentation equipment for the output of graphs and printed data. A multiprogrammer is used for data acquisition and is controlled by computer through an IEEE-488 interface bus. The data acquisition system comprises an input channel multiplexer which can be configured as either 16 single-ended input or 8 differential input channels; and a 12-bit high speed A/D converter with four switch selectable input ranges, namely ± 100 mV, ± 1 V; ± 10 V and ± 100 V. The maximum conversion rate is 33 kHz. The real-time signal processing includes digital filtering, integration (for dose calculations), adaptive sampling, and reflectivity calculations. The output data can be presented in either tabular form (by a printer) or graphically. A graph of any two parameters (R versus D , for example) can be produced during the implantation. Graphical presentation of other relevant data can be obtained after the implant.

A. The Optical System

A general view of the optical system is shown in Fig. 2(a). The picture shows a stainless steel Faraday cup (30 cm long and 10 cm in diameter) which is attached to the existing end station of the ion implantation apparatus, and a dark box to which a laser is connected. This box contains the main optical and the related electronic components. Details are shown schematically in Fig. 2(b). It should be noted that Fig. 2(a) presents a side view, while the drawing of Fig. 2(b) presents a top view (except for the infrared (IR) temperature measurement tube which is

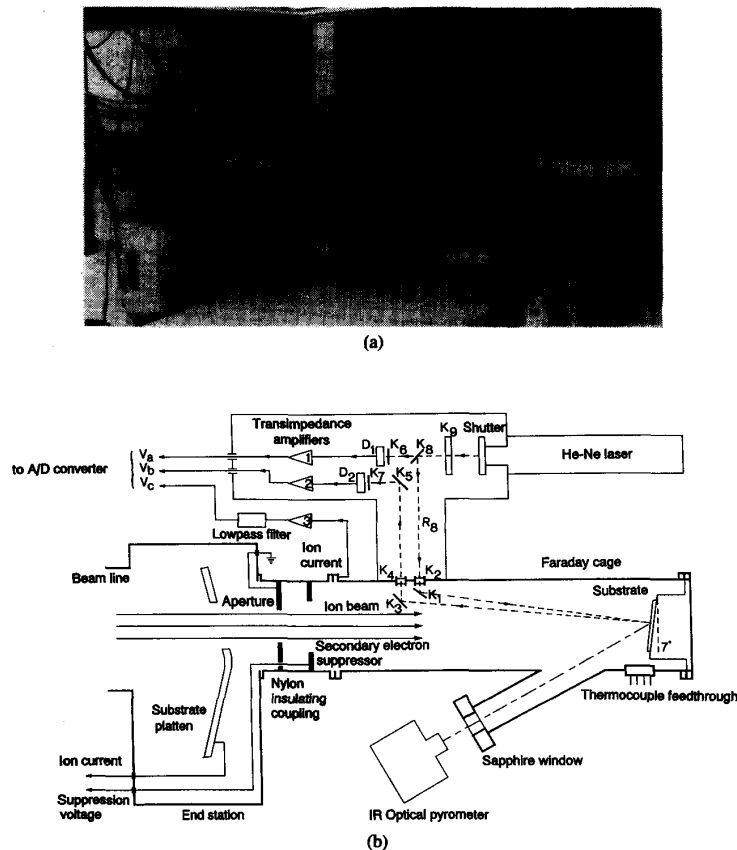


Fig. 2. In-situ optical reflectivity measurement system. a) Side view. b) A detailed top view drawing.

located at the top and not at the side as can be seen from Fig. 2(a). Two mirrors, K_1 and K_3 , are positioned at the appropriate angles and distances from the new position of the substrate holder in order to achieve near-normal incidence to the substrate surface by the probing laser beam. The substrate is tilted 7° with respect to the ion beam to minimize channeling effects, and the angle of incidence of the laser beam is less than 5° with respect to the surface normal. The incident and reflected laser beams pass in and out of the Faraday cup via optical windows K_2 and K_4 , respectively. The average ion beam density arriving at the substrate is determined by the beam current, I , and the aperture with area A , which is formed in a Si-coated aluminum disc. The RF-sputtered silicon coating (thickness approximately $0.5 \mu\text{m}$) is necessary to ensure that no aluminum atoms will arrive to the substrate. This disc is located at the entrance to the Faraday cup which is connected to a vacuum tight insulating nylon flange. The insulation of the Faraday cup from the existing end station enables the measurement of the ion beam current arriving at the new substrate position. Since the Al substrate holder is connected directly to the Faraday cup, the ion beam current signal is obtained from the Faraday cup. This signal is connected to a transimpedance

amplifier (3) which converts it to a voltage signal, V_c . Since the ion beam scans the substrate surface, a low pass filter is required at the amplifier output to smooth the signal. V_c then connects to an A/D converter. To obtain the dose value, the sampled voltage signal is integrated. The details of calibration and computer software will be given later on. Secondary electrons are suppressed to minimize errors in the ion beam current signal and hence in the dose measurements. This is done by means of a circular conductive disc of aluminum located in the nylon insulating coupling and which is connected to a negative potential. The size and the distance of the disc from the substrate are such that low energy electrons emitted from the substrate surface are repelled. Finally, two temperature measuring facilities are provided to enable quantitative high temperature implantation experiments. The first is a direct measurement by means of a thermocouple (not shown) at a point on the interface between the sample and the substrate holder. The second is a noncontact temperature measurement by means of a radiation thermometer which senses the infrared radiation emitted from the substrate surface. The electrical output of this instrument is linear with temperature. The instrument readout is corrected for both emittance and viewing angle. The

radiation is sensed via a sapphire window which is transparent in the infrared wavelength range used by the pyrometer. Both these temperature readings are transferred to the A/D converter to enable control of the substrate temperature by a closed-loop system.

The second main part of the *in situ* optical reflectivity measurement system consists of a closed dark box which includes the aperture for the laser beam, other optical components, photodiodes and amplifiers. The light source used is a He-Ne laser with a wavelength $\lambda = 632.8$ nm. The nominal beam diameter at the $1/e^2$ points is 0.88 mm. The beam divergence is 1 mrad. The nominal power output is 0.4–0.76 mW and the actual measured output is 0.6 mW. The beam is attenuated by a neutral density filter at the laser output (K_9) located close to the output shutter of the laser. In addition, attenuators K_6 and K_7 were attached to the front surfaces of photodiodes D_1 and D_2 . These diodes are Schottky barrier silicon photodiodes. The attenuation was adjusted to prevent saturation of the transimpedance amplifiers at the outputs of the photodiodes. Each of the detectors are covered except for a small aperture such that the laser beam will reach the same point on the photodiode surface, to ensure the same measurement conditions for all the samples. The above coverage also reduces stray radiation from reaching the diode surface. For the wavelength of the He-Ne laser the nominal responsivity is $0.27 \mu\text{A}/\mu\text{W}$ which is in the flat region of the spectral response. With the above conditions, a linear relationship exists over a wide range between the output photocurrent and the incident beam power. The output photocurrents of the diodes are delivered to the input of transimpedance amplifiers 1 and 2 which convert the output currents to voltage signals V_a and V_b , respectively. Their amplification is different to ensure comparable output voltage levels because the light intensity teaching D_2 is lower than that for D_1 as a result of the losses due to the substrate reflectivity and the larger number of components in the optical path. The amplifiers are identical except for a feedback resistor in the second stage. It serves to adjust the required calibration values of voltages V_a and V_b . K_1 , K_3 , and K_5 are multilayered dielectric mirrors. They were specially fabricated for this system and are optimized for high reflectivity at 632.8 nm. K_8 is a 3 dB beam splitter which is also optimized for 632.8 nm.

B. Calibration and Initialization

The output voltages V_a and V_b of amplifiers 1 and 2, respectively, are proportional to the light intensities reaching the diode surfaces. The ratio of these voltages is proportional to the fraction of the laser output light in the direct path through the beam splitter (T_8), and the light reflected from the substrate and attenuated by the various optical components indicated in Fig. 2(b), respectively. In addition, the output voltages, V_a and V_b , include offset components V_1 and V_2 , respectively, which represent the amplifier output signals when the laser beam is blocked off by the shutter. V_1 and V_2 therefore represent the

voltage generated by internal noise, amplifier offset voltage, and by stray radiation reaching the diodes from within the dark box system. These offsets should be determined for a particular system configuration. It is easily measured during initialization before each measurement cycle.

Since the reflectivity is proportional to the ratio of V_b to V_a , it implies that a proportionality constant K , which represents the attenuation through the system, should be defined and its value determined before each measurement cycle. By using the ratio of V_b to V_a , errors which might occur due to changes in the laser output power, P , are eliminated to a large extent. In the case of drift in the laser power, the incident and reflected light will change in the same proportion, and by taking the ratio its influence is reduced. V_a and V_b are given by

$$V_a = PK_9T_8K_6A_1 + V_1 = B_1P + V_1 \quad (1)$$

$$\begin{aligned} V_b &= [P(K_9R_8K_2K_1)][R(K_3K_4K_5K_7)]A_2 + V_2 \\ &= B_2RP + V_2. \end{aligned} \quad (2)$$

The first term in square brackets of (2) represents the beam intensity reaching the sample, while the second term in square brackets denotes the beam intensity reflected from the sample. The K 's, T 's, and A 's represent the attenuation by each of the components in the optical path. A_1 and A_2 included the responsivity of the photodiodes, as well as the transimpedance gain of the amplifiers. By using (1) and (2) the reflectivity can be expressed as

$$R(i) = \frac{B_1 V_b - V_2}{B_2 V_a - V_1} = K \frac{V_b(i) - V_2}{V_a - V_1}. \quad (3)$$

In (3), i indicates the parameter which changes during implantation; therefore $R(i)$ is the reflectivity as a function of the implantation parameter under investigation (e.g., dose, substrate temperature, etc.). In (3) only V_b is a variable which is related to the implant. It is also noted that P , the laser output power, is cancelled in (3). Therefore, if the offset voltages V_1 and V_2 were zero, the reflectivity would be directly proportional to the ratio V_b/V_a . By having little stray light, it is ensured that $V_1 \ll V_a$ and $V_2 \ll V_b$. The final calibration step is the determination of the system proportionality constant, K . According to (3), $K = B_1/B_2$. (1) and (2) show that B_1 and B_2 are system constants which depend on the attenuation by the optical components of the system and the amplifier gain. A sample of known reflectivity, say R_0 , is placed in the system and the voltages V_a , V_b , V_1 and V_2 measured. The constant K is then calculated from (3):

$$K = R_0 \frac{V_{a0} - V_{10}}{V_{b0} - V_{20}} \quad (4)$$

where the zero subscripts indicate the voltage values obtained for a reference sample with known reflectivity, which is typically that of an unimplanted sample. The value of K obtained by applying (4), remains the constant

for the same sample under various implantation conditions.

V_a and V_b provide information relevant to the optics of the system to the computer. A third voltage, V_c , which represents the ion beam current signal is used to calculate the implanted dose rate. This voltage is obtained by an analog current-to-voltage converter with

$$V_c = \frac{1}{S}I + V_3 \quad (5)$$

where V_3 is an offset voltage produced at the output of the converter for zero beam current. S is the voltage-to-current conversion factor measured in A/V . The value of S is determined experimentally by measuring V_c and V_3 for a known beam current I_0 on a dummy wafer. It follows from (5) that:

$$S = \frac{I_0}{V_{c0} - V_{30}} \quad (6)$$

where V_{c0} and V_{30} denote voltages obtained for a beam current I_0 . This value of S is then used throughout the measuring cycle.

To summarize, calibration and initialization of the system imply the experimental determination of the offset voltages V_1, V_2, V_3 , and the constants K and S . The offset voltages are determined by blocking the incident and reflected laser beams from reaching D_1 and D_2 and stopping the ion beam current from reaching the substrate, respectively.

After initialization, the measurands V_a, V_b , and V_c are transferred to the data acquisition system where the data is sampled at predetermined points in time. From this data a graph of e.g., R versus D can be constructed using (3) and (5). By keeping all the implant conditions constant, R versus D measurements (or versus any other parameter) can be obtained with a predetermined number of sampling points per decade of dose. Practically, this means that the time interval between each set of the above data is adjusted automatically to distribute the data points evenly within each decade. For example, the same number of data points are allocated to the dose range of 10^{14} – 10^{15} cm^{-2} and 10^{15} – 10^{16} cm^{-2} , respectively. In our system the total number of sampling points, N , was 2048. The system is also self-adaptive, i.e., the system has a time dependent sampling rate which is inversely proportional to the actual calculated dose at the instant of sampling. When, for example, for some unexpected reason the ion beam current changes during the implant, the sampling rate is adjusted to keep the number of data points sampled per decade of dose, constant. The maximum sampling rate is limited by the conversion speed of the A/D converter, and the maximum number of available data points, N , is limited by the available memory of the computer system.

The implanted dose per unit area, D , is calculated by integrating the number of ions carried by the beam and

reaching a unit area of the substrate

$$D[\text{cm}^{-2}] = \frac{1}{qA} \int_0^t I dt. \quad (7)$$

In our case the integration is done by computer, and I is proportional to V_c . It follows from (5) and using the trapezoidal approximation of integration, that the dose at sampling point n , is given by

$$D(n) = \frac{S}{2qA} \sum_{i=0}^n [V_c(i) + V_c(i+1) - 2V_3] \Delta t(i). \quad (8)$$

This expression for dose may be written in a form which can be computed iteratively, namely

$$D(n) = D(n-1) + \frac{S}{2qA} [V_c(n) + V_c(n+1) - 2V_3] \cdot [t(n+1) - t(n)]; \quad n = 1, 2, \dots, N \quad (9)$$

where

$$D(0) = \frac{S}{2qA} [V_c(0) + V_c(1) - 2V_3] [t(1) - t(0)]. \quad (10)$$

Software controls the initialization and calibration of the reflectometer as well as the sequencing of the data acquisition and the final data processing and presentation. A flow diagram of the program is shown schematically in Fig. 3. For the initialization procedure the implant energy, aperture, reflectivity of a reference sample, the beam current, the maximum dose required, and the maximum number of data points to be acquired, are used as inputs. The system calibration is performed as described previously. System constants, namely the beam current factor, S , and the reflectance factor, K , are calculated from the data acquired during the initialization procedure. These values are saved on magnetic media for future reference.

After completion of the setup procedure, data capturing can be started. This is done by triggering the multiplexer and the A/D converter at intervals predetermined by the maximum dose required, the ion beam current and the maximum number of data points to be sampled. The sampled analog values are then converted to digital numbers and saved in the form of a matrix. The time interval between two subsequent sets of measurements is calculated to space the available data points equally on a logarithmic time scale proportional to the implanted dose. This time interval is also changed automatically to compensate for a change in the ion beam current. Data capturing is ended when the maximum preset dose is reached or when the maximum allowed number of data points has been captured. From the four acquired sets of data $V_a(n), V_b(n), V_c(n)$, and time $t(n)$, $n = 1, 2, \dots, N$, together with the system constants and other values measured during the initialization procedure, the dose versus reflectivity curve is calculated. After completion of the implant, the sets of data are saved.

III. EXAMPLES

Some experimental examples are now presented to demonstrate the type and quality of the output informa-

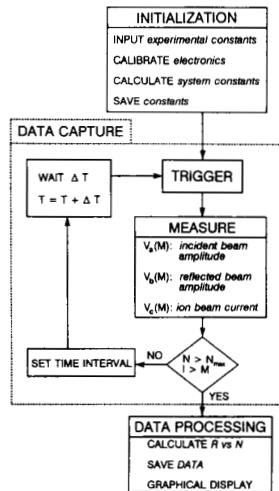


Fig. 3. Software flow diagram.

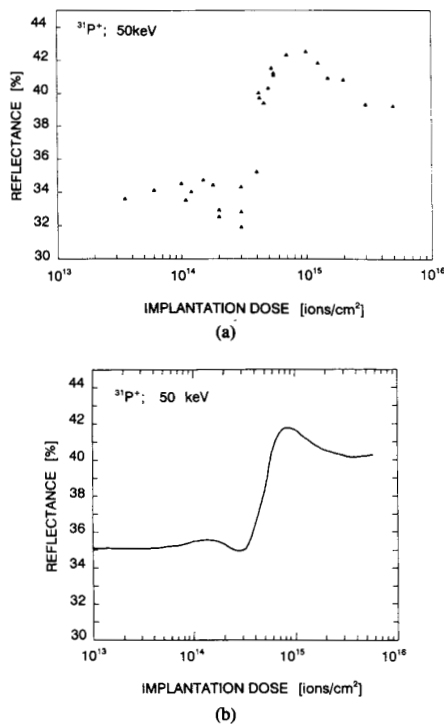


Fig. 4. Reflectivity versus dose results for 50 keV $^{31}\text{P}^+$ silicon implanted single crystal (111) substrate. a) Graph constructed by discrete points each representing post implantation reflectivity of one sample, for certain dose. b) Continuous graph obtained of one sample by *in situ* reflectometry showing the changes in R for various doses for that sample.

tion generated. Fig. 4(a) presents the R versus D graph obtained by using the multiple sample approach of constructing curves by using several samples (27 in this case) each implanted to a different dose and with the reflectivity measured outside the target chamber. As a result, each

sample yields one data point on the graph. Fig. 4(b) shows a similar, but continuous graph obtained using only one sample. The differences are clear and relate to the advantages cited in the introduction. We want, however, to emphasize two points here. The first concerns the most important part of the graphs, namely the region where a steep change in R occurs within a small change in the implanted dose. Constructing this region on the graph in Fig. 4(a) proved to be difficult, because it is hard to distribute the data points evenly in such a small dose range if one has no *a priori* knowledge of where it will occur. As a result many data points of this region in Fig. 4(a) are located at the higher reflectivity part of the region leaving the lower part practically empty. The second point concerns the fine detail on the curve of Fig. 4(a) which is hardly observed. These shortcomings are overcome in Fig. 4(b). As a result, interference patterns, slopes, maxima, minima and points of inflection can be determined to give information about the implant process.

Figs. 5 and 6 show results obtained by the automated system for the implantation of N_2 and Ar ions, respectively. Apart from typical R versus D curves presented for each case, the two figures given in part (c) of each graph, depict the ion beam current as a function of dose. Fig. 5(c) represents a fairly stable ion beam current and Fig. 6(c) represents a fairly unstable ion beam current. The point to be made here is that once the changes in the ion beam current are known in conjunction with the changes in reflectivity, one can investigate the effects, as a case history. Fig. 5(b) and 6(b) present the voltage signals which represent the light intensities of the reference and reflected beams as a function of time. The ratio of the above signals (corrected for the offset voltages) yields the reflectivity. Again, it is observed that the intensity of the reference beam is not constant due to statistical variations, but since a single light source is used, coherent statistical deviations occur in the reflected beam which are superimposed on the changes occurring as a result of the changes in the material, the ratio of V_b to V_a will drastically reduce the noise. Subsequent digital filtering of the reflectance curve may reduce the noise even further. Fig. 7 demonstrates other possibilities of measured data presentation i.e. of ion beam current 7(a) and implanted dose 7(b) as a function of implantation time.

Finally, it should be noted that the above examples relate the reflectivity to the implanted dose either directly (R versus D graphs) or indirectly, as shown. Reflectivity, however, can be related in a similar way to other parameters such as ion beam energy, substrate temperature, etc, to obtain other desired trends. Other possible potential applications are listed below.

IV. OTHER APPLICATIONS

The advantages of the *in situ* measuring system are mainly concerned with monitoring the reflectivity changes by data acquisition and signal processing. The system capabilities, however, can be expanded to include other applications which could advance both research and man-

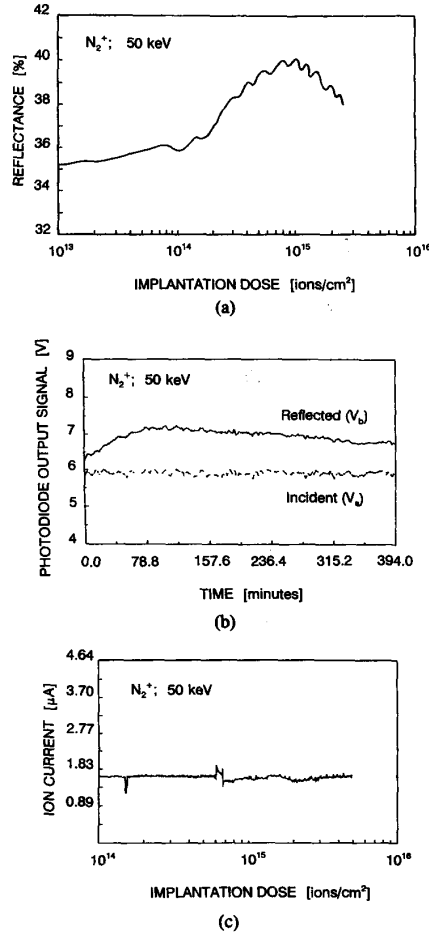


Fig. 5. N_2^+ implantation a) Continuous R versus D graph. b) Processed signal of the reference and reflected beam intensities, as a function of implantation time. c) Beam current as a function of implantation dose.

ufacturing. Some of these applications are mentioned briefly below.

A. Process Control: Since the implantation process parameters are monitored continuously, the information is obtained in a real-time fashion. The signals received from both the changes in R and the simultaneously monitored changes in the implantation conditions, such as dose, energy, ion beam current and uniformity, can be used to control the process parameters as the implant progresses. This can be done by closing feedback loops to obtain desired online adjustments, which either stabilize the implantation conditions to constant values or change them according to some predesigned programs. An important feature of such an *in situ* monitoring system, is the possibility of optical scanning of the substrate during implantation, to determine whether or not some lateral inhomogeneities of reflectivity exists which will indicate uneven lateral implantation. Such on-line real-time information can be used to guide the implantation system by adjusting, for example, the ion optics to yield homogeneously im-

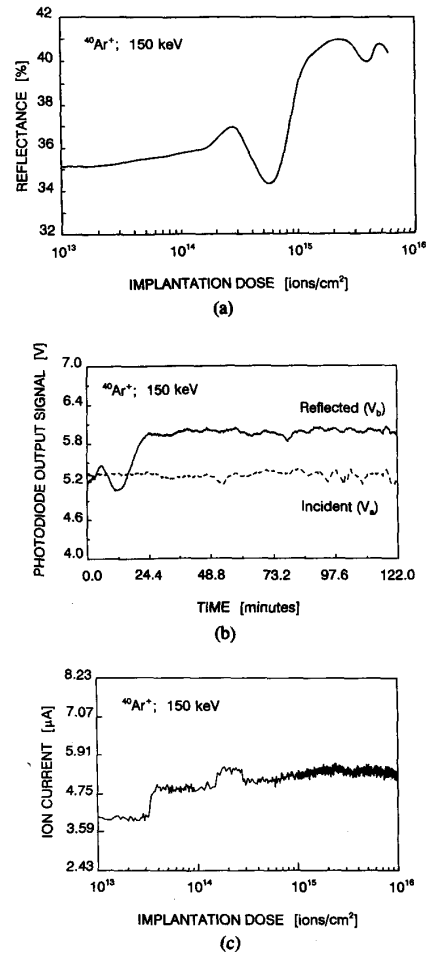


Fig. 6. Ar^+ implantation (150 keV). a) Continuous R versus D graph. b) Processed signals of the reference and reflected beam intensities, as a function of implantation time. c) Beam current as a function of implanted dose.

planted surfaces, or if needed, to deliberately produce inhomogeneous implants in selected areas. This type of control could result in more accurate and repeatable results.

B. In situ detection of abnormalities: Quality control can be introduced by *in situ* monitoring of the reflectivity to detect any significant unexpected changes which extend beyond the limits of the predetermined parameter spread. These abnormalities could occur as a result of, e.g., high lateral temperature gradients caused by uneven heating of the substrate by the ion beam. With *in situ* monitoring of the process parameters and the reflectivity, the implant can be terminated prematurely should something go wrong. This is in contrast to the *ex situ* methods, by which one can detect abnormalities only after the entire process has been completed.

C. Data Base: The data acquired during the implant is saved on magnetic media. A data base with such informa-

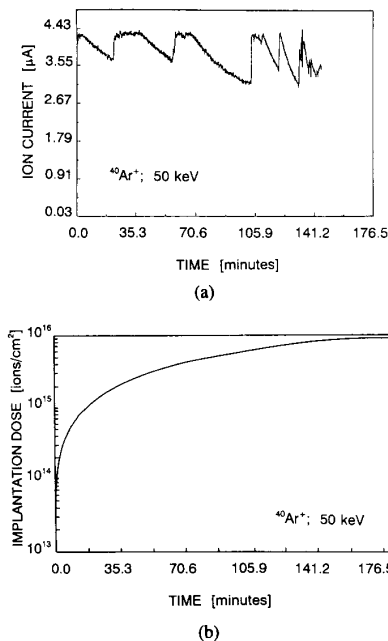


Fig. 7. Ar^+ implantation (50 keV). (a) Ion beam current vs implantation time. (b) Implanted dose vs implantation time.

tion can be used for repeating, analyzing and improving the process. The data can be processed and important critical points on the graph such as maxima, minima, points of inflection, slopes, rates, etc., can be computed. This information could be used to explain physical changes occurring in the implanted materials. A case history of each individual implanted substrate would then be available if needed. Any desired part of the R versus any implantation parameter graphs could be expanded and zoomed in to for a detailed study.

D. Mapping: Since the optical scanning is in principle *in situ*, spatial and time dependent mapping of the surface reflectivity could be obtained. This information could be used to determine the uniformity of the implant over the surface of the substrate.

E. In-Situ Annealing: The optical system enables one to monitor *in situ* annealing as well. In the case of annealing, reordering of the atoms in the damaged layer created within the substrate during implantation, affects new changes of the reflectivity. As the annealing progresses the reflectivity is reduced towards its original unimplanted value. The *in situ* probe would then serve as an end-point detector. The advantage of performing the anneal process within the implantation chamber is that it is performed in a clean high vacuum environment, minimizing the penetration of undesirable contamination, and the formation of oxide layers as is the case when annealing in atmospheric pressure systems. The possibility for rapid thermal annealing exists as well, since the flashes of the annealing light source can be continued until the *in situ* reflectivity monitor indicates the appropriate value of reflectivity [1].

V. SUMMARY

The system performance advantages and applications of the continuous *in situ* monitoring of the optical reflectivity are of significant practical importance. This could be achieved for a relatively small investment. As a result it constitutes a powerful analytical and diagnostic tool which provides reliable, consistent and reproducible means for the evaluation of the structural changes which take place within the implanted substrate while it is actually occurring.

VI. ACKNOWLEDGMENT

The authors wish to express their gratitude towards the Foundation for Research Development and Rand Afrikaans University for the research grants which enabled them to perform the work.

REFERENCES

- [1] G. L. Olson and J. A. Roth, "Kinetics of solid phase crystallization in amorphous silicon," *Mater. Sci. Rep.*, vol. 3, pp. 1-78, 1988.
- [2] P. L. Swart, B. M. Lacquet, and H. Aharoni, "In-situ measurement of crystalline-amorphous transition in Si substrate during ion implantation," *IEEE Trans. Nucl. Sci.*, vol. 39, pp. 464-467, 1992.
- [3] H. Aharoni and P. L. Swart, "Changes in the optical reflectivity of implanted silicon as a function of implantation energy," *Appl. Phys. Lett.*, vol. 44, pp. 892-894, 1984.
- [4] P. L. Swart, H. Aharoni, and B. M. Lacquet, "Optical reflectometry of radiation damage in ion implanted silicon," *Nucl. Instr. Meth. Phys. Res.*, vol. B6, pp. 365-371, 1985.
- [5] P. L. Swart, B. M. Lacquet, and M. F. Grobler, "In-situ reflectance measurements of semiconductors during ion-implantation," *Materials Research Society Symposium Proceedings*, vol. 147, pp. 119-124, 1989.
- [6] P. L. Swart, B. M. Lacquet, and H. Aharoni, "An experimental investigation of amorphization of silicon during phosphorus ion implantation by in-situ optical reflectance measurements," presented at the Seventh International Conference on Ion Beam Modification of Materials (IBMM-1990), Knoxville, Tennessee, September 9-14, 1990.
- [7] H. Aharoni, P. L. Swart, and B. M. Lacquet, "Some characteristics of crystalline-amorphous threshold point of $^{31}\text{P}^+$ ion-implanted silicon substrates," *IEEE Trans. Nucl. Sci.*, vol. 38, pp. 976-978, 1991.
- [8] G. E. Aizenberg, P. L. Swart, and B. M. Lacquet, "Optical characterization of semiconductors containing inhomogeneous layers," vol. 63, pp. 249-254, 1993.
- [9] G. E. Aizenberg, P. L. Swart, and B. M. Lacquet, "A digital signal-processing analysis technique for the infrared reflectivity characterization of ion implanted silicon," *J. Electron. Mat.*, vol. 21, pp. 1033-1040, 1992.
- [10] G. K. Hubler, P. R. Malmberg, C. N. Waddell, W. G. Spitzer, and J. E. Fredrickson, "Electrical and structural characterization of implanted doped silicon by infrared reflection," *Rad. Effects*, vol. 60, pp. 35-47, 1982.
- [11] R. E. Hummel, W. Xi, and D. R. Hagman, "Ion implantation damage and annealing of silicon as characterized by differential reflectometry," *J. Electrochem. Soc.*, vol. 137, pp. 3583-3588, 1990.
- [12] V. I. Stavrov, R. Varbanov, O. Vasiliev, and D. Berova, "Investigation of arsenic-implanted silicon by optical reflectometry," *Vacuum*, vol. 42, pp. 107-109, 1991.
- [13] T. M. Burns, S. Chongsawangvirod, J. W. Andrews, E. A. Irene, G. McGuire, and S. Chevacharocukul, "A comparison of the measurement of ion damage in silicon surfaces using differential reflectance and spectroscopic ellipsometry," *J. Vac. Sci. Technol.*, vol. B9, pp. 41-49, 1991.
- [14] M. Holtz, R. Zallen, O. Brafman, and S. Matteson, "Raman-scattering depth profile of the structure of ion-implanted GaAs," *Phys. Rev. B.*, vol. 37, pp. 4609-4617, 1988.
- [15] J. E. Fredrickson, C. N. Waddell, W. G. Spitzer, and G. K. Hubler, "Effects of thermal annealing on the refractive index of amorphous silicon produced by ion implantation," *Appl. Phys. Lett.*, vol. 40, pp. 172-174, 1982.

- [16] S. Prussin, D. I. Margolese, and R. N. Tauber, "Formation of amorphous layers by ion implantation," *J. Appl. Phys.*, vol. 57, pp. 180-185, 1985.
- [17] M. K. El-Ghor, O. W. Holland, C. W. White, and S. J. Pennycook, "Structural characterization of damage in Si(100) produced by MeV Si⁺ ion implantation and annealing," *J. Mater. Res.*, vol. 5, pp. 352-359, 1990.
- [18] K.-W. Wang, W. G. Spitzer, G. K. Hubler, and D. K. Sadana, "Ion implantation of Si by ¹²C, ²⁹Si and ¹²⁰Sn: amorphization and annealing effects," *J. Appl. Phys.*, vol. 58, pp. 4553-4564, 1985.
- [19] R. R. Hart and O. J. Marsh, "Changes of optical reflectivity (1.8 to 2.2 eV) induced by 40-keV antimony ion bombardment of silicon," *Appl. Phys. Lett.*, vol. 14, pp. 225-226, 1969.
- [20] S. Kurtin, G. A. Shifrin, and T. C. McGill, "Ion implantation damage of silicon as observed by optical reflection spectroscopy in the 1 to 6 eV region," *Appl. Phys. Lett.*, vol. 14, pp. 223-225, 1969.
- [21] G. L. Olson, S. A. Kokorowski, R. A. McFarlane, and L. D. Hess, "Direct observation of laser-induced solid phase epitaxial crystallization by time-resolved optical reflectivity," *Appl. Phys. Lett.*, vol. 37, pp. 1019-1021, 1980.
-
-